Sensors & Diagnostics

PAPER

Check for updates

Gate voltage effect on fluorinated and non-fluorinated copper phthalocyanine OTFT-based ammonia sensors

Sofia Gallardo-Pascual, [iD] [a] Benjamin King, [iD] [a] Sujithkumar Ganesh Moorthy[ab] and Benoît H. Lessard [iD] *[ac]

Organic thin-film transistors (OTFTs) have emerged as a promising platform for gas sensing applications due to their low-power operation, room-temperature sensitivity, and structural tunability. In this work, we investigate the effect of gate voltage (V_{GS}) on the ammonia (NH_3) sensing performance of OTFT-based sensors using copper phthalocyanine (CuPc, p-type) and its fluorinated derivative ($F_{16}CuPc$, n-type) as the active layers for the first time. Devices were exposed to NH_3 concentrations ranging from 0 to 100 ppm, and their electrical responses were monitored across different V_{GS} values. Results demonstrate that modulating V_{GS} significantly impacts key sensing parameters, including relative response (RR), sensitivity, limit of detection (LOD), and response/recovery kinetics. The lowest LODs achieved were 0.4 ppm for CuPc and 0.21 ppm for $F_{16}CuPc$. These findings highlight the potential of V_{GS} modulation as a powerful strategy to optimize OTFT sensor performance and provide a new dimension of tunability for gas detection technologies at room temperature.

1. Introduction

Gas-sensing technologies have garnered significant attention in recent years due to their critical role in monitoring and controlling gas leaks, regulating indoor air quality, and managing humidity and CO_2 levels in congregate settings.[1–3] Gas sensors are also widely utilized for the detection of hazardous gases such as ammonia (NH_3), nitrogen dioxide (NO_2), and volatile organic compounds (VOCs), whose measurement is essential for environmental surveillance and occupational health monitoring.[4] Moreover, the development of gas sensor arrays with multivariate data analysis has opened pathways to non-invasive disease diagnostics, representing an emerging frontier in medical sensing technologies.[5] Consequently, the development of gas sensors that are highly sensitive, selective, and low power are critically important for both technological innovation and commercial deployment.

Chemiresistors, typically composed of metal oxide sensing layers, have been widely deployed in gas sensing owing to their simplicity and high sensing performance.[6,7] However,

a Department of Chemical and Biological Engineering, University of Ottawa, 161 Louis Pasteur, Ottawa, ON, K1N 6N5, Canada. E-mail: Benoit.Lessard@uottawa.ca
b Department of Chemistry and Biomolecular Sciences, University of Ottawa, 150 Louis Pasteur, Ottawa, ON, K1N 6N5, Canada
c School of Electrical Engineering and Computer Science, University of Ottawa, 800 King Edward Ave, Ottawa, ON, K1N 6N5, Canada

the elevated operating temperatures of metal oxide sensors required to achieve their optimal performance (>200 °C) poses a major barrier to seamless integration with standard silicon-based technologies[4] and makes them incompatible with low-power electronics.[8] Organic semiconductor-based chemiresistors can operate at room temperature but only have two electrodes, which limits their operational flexibility.[9–12] In contrast, organic thin-film transistor (OTFT) based sensors, which are three terminal devices, are the combination of a sensor and an amplifier, and a slight modulation in gate bias can change the response (signal-to-noise ratio) of the device by several orders of magnitude, which provides the potential for ultra-low limit gas detection at room temperatutes,[4,13–15] Additionally, organic semiconductors offer advantageous properties for sensing technologies, including low fabrication cost and synthetic tunability, which can enhance selectivity and sensitivity.[16]

Recent advancements of OTFT-based gas sensors have largely been driven by three core strategies: the development of novel organic semiconductors with enhanced sensitivity to target gases,[17,18] the systematic modification of interfacial properties between functional layers,[19–21] and the precise control of the microstructural characteristics of the sensing films.[12,13,22] However, the effect of modulating V_{GS} on the sensor performance has been relatively unexplored. Shao *et al.* found that operating a TIPS-pentacene OTFT NO_2 sensor in the sub-threshold region resulted in a 19-fold increase in responsivity compared to operation in the

saturation region.[14] Sato *et al.* demonstrated that the change of the Fermi level by manipulating the gate electric field in a graphene bilayer significantly affects not only the rate of molecular adsorption but also the carrier-scattering strength of adsorbed molecules.[23] However, a comprehensive analysis of the gate voltage effect on other sensor performance metrics, such as sensitivity, limit of detection, response and recovery times is missing from the literature. As the V_{GS} is the principal controller of the charge carrier density, this intrinsic characteristic of the OTFT architecture could justify the choice of this more complicated architecture over a two-terminal device for specific applications.

Herein, we investigate the effect of V_{GS} on the gas sensing performance of OTFT-based NH_3 sensors with p-type organic semiconductor copper phthalocyanine (CuPc) and n-type organic semiconductor copper(II) 1,2,3,4,8,9,10,11,15,16,17,18,22,23,24,25-hexadecafluoro-29H,31H-phthalocyanine (F_{16}CuPc) as the sensing layers. NH_3 was selected as the target analyte due to its critical role across various sectors, including agricultural, pharmaceutical, and biomedical diagnostics,[24] with over 175 million tonnes produced per year.[25] CuPc and F_{16}CuPc have been widely used in gas sensing platforms such as chemiresistors,[26] OTFTs,[27,28] and heterojuctions.[29–31] However, to the best of our knowledge, these results demonstrate the first report of OTFT-based sensors using these materials as the sensing layer for NH_3 sensing. Devices were exposed to concentrations of NH_3 gas from 0 to 100 ppm, and the impact of V_{GS} on sensitivity, limit of detection (LOD), and response kinetics was systematically evaluated. Our approach demonstrates that modulating the operating V_{GS} serves as an effective strategy to enhance the performance of three-terminal gas sensors, and highlights the advantages offered by OTFTs.

2. Materials and methods

2.1 Device fabrication

N-doped Si substrates (Ossila) with a 230 nm thermally-grown SiO_2 dielectric layer were treated following the procedure reported in our previous work.[32] Bottom-gate top-contact (BGTC) OTFTs using CuPc and F_{16}-CuPc as the organic semiconductor were fabricated by thermally evaporating a 50 nm-thick layer at 0.2 Å s^{-1} under vacuum ($P < 2 \times 10^{-6}$ Torr). Substrates were then removed, and a diamond-tipped pen was used to scratch a section of a substrate to yield exposed Si for gate electrode deposition. The substrates were then placed in a source–drain shadow mask ($L = 1$ mm, $W = 65$ μm) purchased from BlueRing. Electrodes were fabricated by thermally depositing a 50 nm-thick layer of Ag at a rate of 1 Å s^{-1} under vacuum ($P < 2 \times 10^{-6}$ Torr) (Fig. 1).

2.2 Gas sensing set up and electrical characterization

A blend of NH_3 and synthetic air (1000 ppm NH_3, purchased from Messer Canada Inc, Canada) was diluted with dry synthetic air using mass flow controllers (total flow: 200 sccm to reach stable, controlled and adjustable ammonia concentrations from 0 to 100 ppm) prior to being mixed and introduced to a testing chamber containing the device under test. The final concentration of the gas and the relative humidity was controlled and monitored using a custom Labview program. The electrical characterization of the sensor was performed with a custom-built auto tester and a Keithley 2614B source meter previously reported by our group,[32] allowing us to set the gate–source voltage and source–drain voltage (V_{SD}) while measuring the source–drain current (I_{DS}) in the device under test. The autotester was directly connected to the testing chamber, with autotester probes directly contacting the source, drain, and gate electrodes. For gas sensing experiments, the V_{GS} and V_{DS} were maintained constant while recording the I_{DS} under different NH_3 concentrations. Transfer and output curves were measured firstly under synthetic air, followed by measurements at different ammonia concentrations. Transfer curves were measured with the gate voltage sweeping between −10 and 45 V for F_{16}CuPc and from 10 to −45 V for CuPc based devices, both with a step size of 0.45 V, and a source–drain voltage (V_{DS}) of 45 V and −45 V, respectively. Output
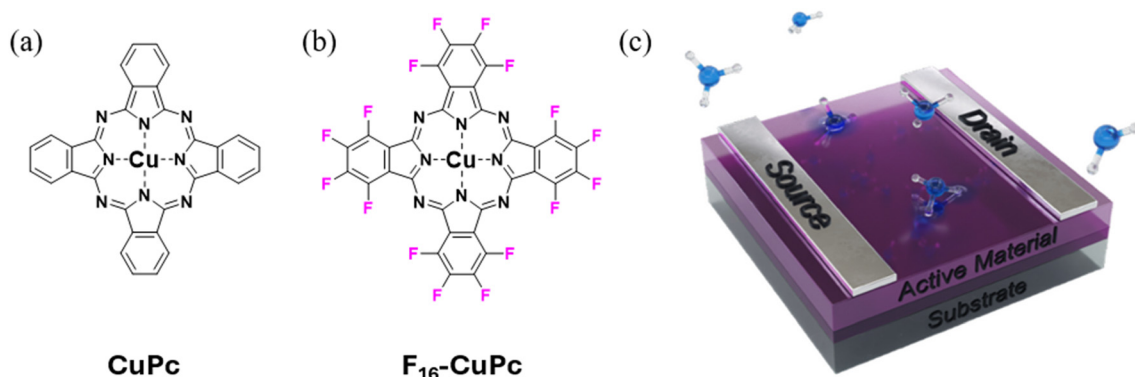

Fig. 1 Molecular structure of a) CuPc and b) F_{16}CuPc, and c) the OTFT sensor device scheme.

curves were measured using a V_{DS} ranging between 45 and 0 V and V_{GS} varying from 0 to −45 V, with a step of 5 V and −5 V for $F_{16}CuPc$ and CuPc respectively. The threshold voltage (V_{th}) and mobility (μ) were calculated from the transfer curves at the saturation regime using eqn (1):

$$I_{ds} = \frac{\mu C_i W}{2L}\left(V_{GS} - V_{th}\right)^2 \qquad (1)$$

where C_i is the capacitance of the dielectric layer, and L and W represent the length and width of the channel, respectively.

3. Results and discussion

3.1 Effect of NH₃ on F₁₆CuPc and CuPc OTFT-based sensors performance

The transfer and output curves of the CuPc and $F_{16}CuPc$ OTFTs measured under ambient conditions are shown in Fig. 2a–c and exhibit electrical characteristics consistent with previous research.[27] $F_{16}CuPc$ has a (n-type) mobility of

0.02 cm V^{-1} s^{-1} and a V_{th} of 6.8 V and CuPc has a (p-type) mobility of 0.01 cm V^{-1} s^{-1} and a V_{th} of 6.4 V.

3.2 The operational V_{GS} effect on the F₁₆CuPc and CuPc OTFT-based sensor's performance metrics

Devices were exposed to different concentrations of NH₃ varying from 0 to 100 ppm at a fixed flow rate of 200 sccm. *In situ* measurements of the transfer and output curves were taken using an exposure time (under NH₃) of 2 minutes at each step in concentration with a recovery time (under synthetic air) of 4 minutes. For CuPc sensors, I_{DS} decreases accompanied by a shift in V_T, under exposure to NH₃ and increases during the recovery period (Fig. 3a and b). The log plots of the transfer curve more clearly highlight the shift in the V_T (Fig. 3b). These observations are consistent with p-type behaviour where NH₃ molecules donate electrons to the CuPc film, resulting in a depletion of holes and a decrease in I_{DS}. This is consistent with previously-reported CuPc chemiresistors, which demonstrated p-type behaviour when exposed to NH₃.[28] In contrast, I_{DS} increases upon exposure to NH₃ for $F_{16}CuPc$ OTFT devices (Fig. 3d) with a shift in V_T
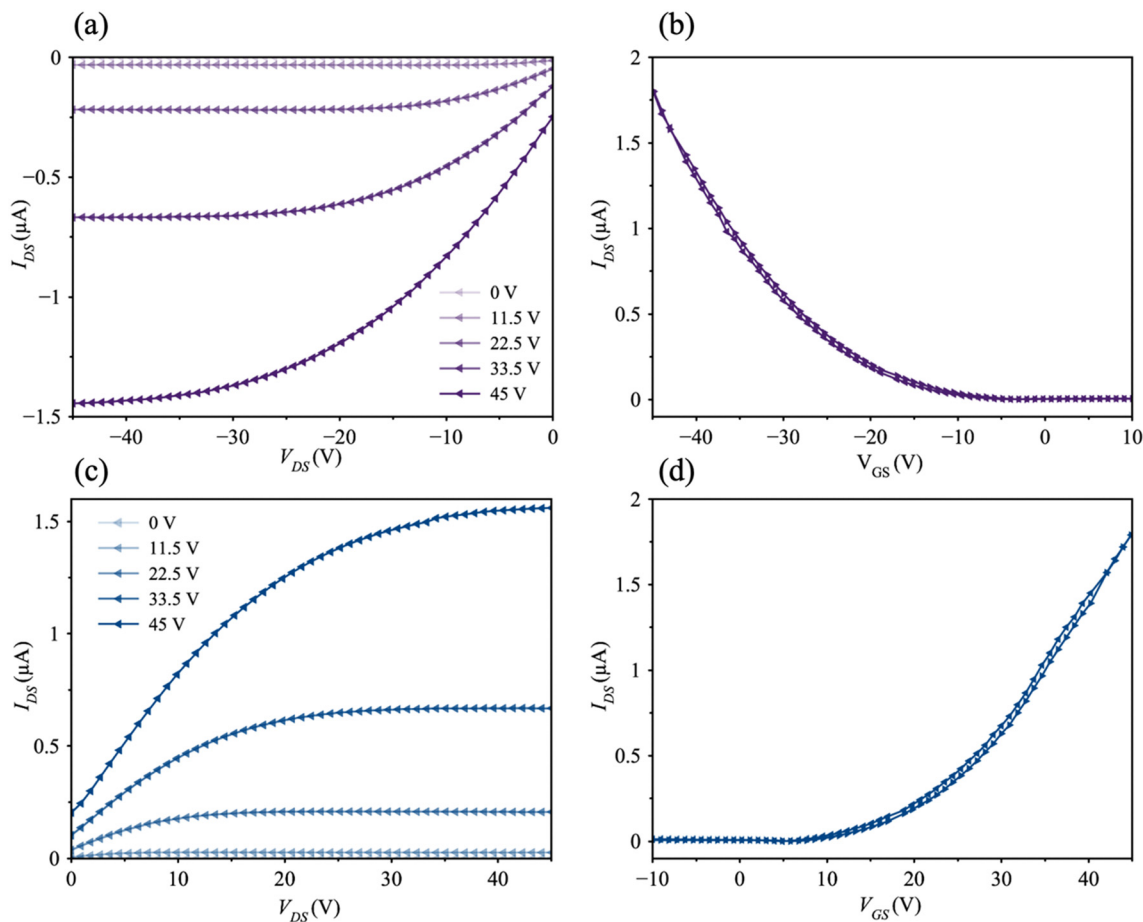

Fig. 2 Output and transfer characteristics of CuPc (a and b) and F₁₆CuPc (c and d) OTFTs. Transfer curves were measured at V_{DS} = −45 V for CuPc and V_{DS} = 45 V for F₁₆CuPc, with V_{GS} swept from 10 to −45 V and −10 to 45 V, respectively. Output curves were measured at V_{GS} of (0, −11.5, −22.5, −33.5 and −45) for CuPc and (0, 11.5, 22.5, 33.5 and −45) for F₁₆CuPc.
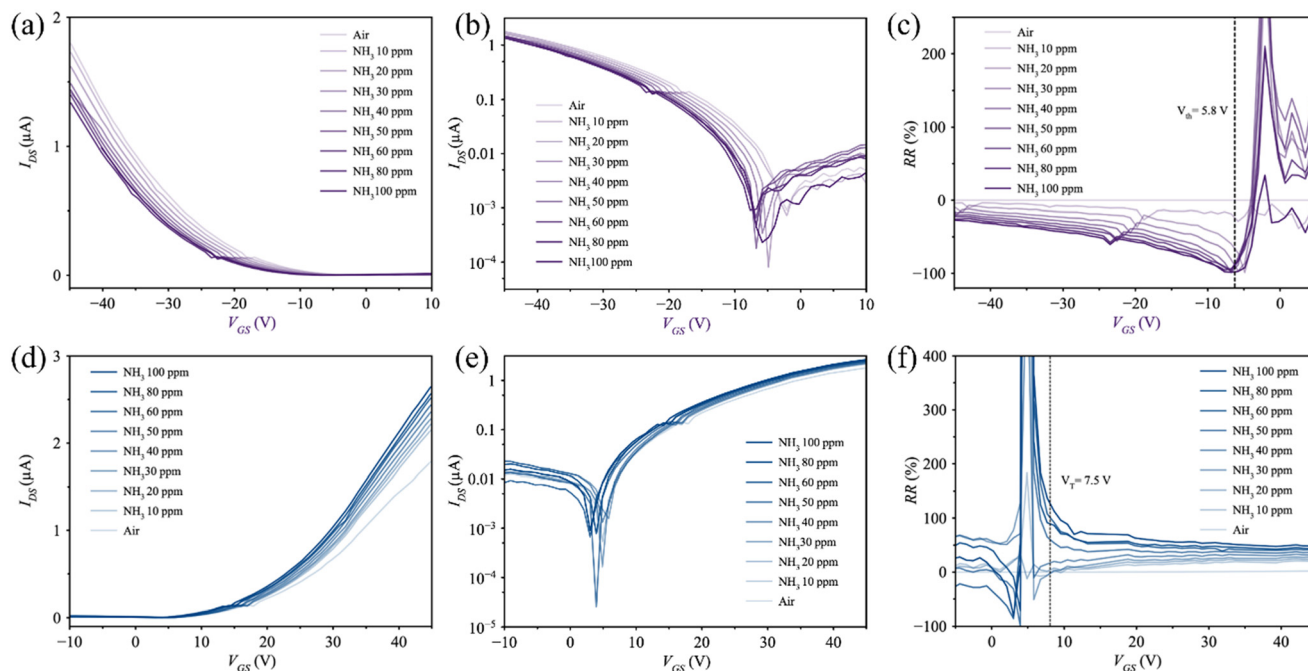
Fig. 3 Transfer curves at different ammonia concentrations of CuPc: a) linear plot and b) log plot, and $F_{16}CuPc$: d) linear plot and e) log plot. The relative response as a function of gate voltage for c) CuPc and f) $F_{16}CuPc$ OTFTs as a function of ammonia concentrations.

(Fig. 3e), which is consistent with n-type behaviour, where an increase in electron carrier density in the film results in an increase in I_{DS}.

The relation between the RR of the sensor and V_{GS} was established by plotting RR as a function of V_{GS} across the NH_3 concentrations we measured in this work (Fig. 3c and f). RR was calculated using eqn (2);[33]

$$RR\% = \frac{I_f - I_0}{I_0} \times 100 \qquad (2)$$

where I_f and I_0 are the final and initial current values for each concentration. To plot the RR across all V_{GS} values, the I_f is equal to the transfer curve taken at the corresponding NH_3 concentration and I_0 is the transfer curve taken under synthetic air. By doing this, it is easier to visualize how the RR under the same NH_3 concentration can be increased or decreased by operating the OTFT-based sensor on a different V_{GS} value.

For CuPc devices, the RR is negative, while for $F_{16}CuPc$, the RR is positive, which is consistent with the n-type and p-type behaviour shown before. For both materials, the highest RR is observed in the subthreshold region and is attributed to the filling of charge traps by the majority charge carriers.[34] Despite the high RR values in this region, 12 000% for $F_{16}CuPc$ and 4000% for CuPc, RR begins to behave linearly beyond the subthreshold region of the transfer curves. For CuPc, the RR increases at lower V_{GS} for all measured NH_3 concentrations. The impact of the V_{GS} on the RR was more prominent at low NH_3 concentrations (10 ppm), where the RR increased from −3.5% to −18% when the V_{GS} was decreased

from −43 V to −8.6, compared to high concentrations (100 ppm), where the RR increased from −27% to −97% when the V_{GS} was equally decreased. For $F_{16}CuPc$, the effect of the V_{GS} on the RR is more dependent on the NH_3 concentration. For low concentrations (10 ppm) the RR is decreased when operating at lower V_{GS} but for high concentrations (100 ppm) it shows the opposite behaviour. These findings show the potential to optimize the sensor RR for specific NH_3 concentration windows by tuning the V_{GS}.

3.3 Dynamic measurements of the OTFT-based sensors

High sensitivity and low LOD are critical for evaluating the performance of OTFT-based ammonia sensors. To investigate the impact of gate voltage V_{GS} on the dynamic response, we exposed the devices to NH_3 concentrations ranging from 10 to 100 ppm, using 1-minute exposure and 4-minute recovery cycles. Measurements were performed at a constant drain-source voltage of +45 V for $F_{16}CuPc$ and −45 V for CuPc, while systematically varying V_{GS}. Notably, all the V_{GS} measurements were performed on the same day in the same sensor to be able to compare the results. Fig. 4a–f presents the time-resolved drain current under increasing NH_3 concentrations at different V_{GS} values. The sensitivity of each device was extracted from calibration curves, defined by the RR *versus* concentration. A clear trend emerged: both CuPc and $F_{16}CuPc$ exhibited decreasing sensitivity at higher V_{GS} values. In the case of CuPc OTFT sensors, a nonlinear and undetectable response at lower concentrations (10–20 ppm) was observed when operating at V_{GS} = −45 V. However, at V_{GS} = − 36 V, the
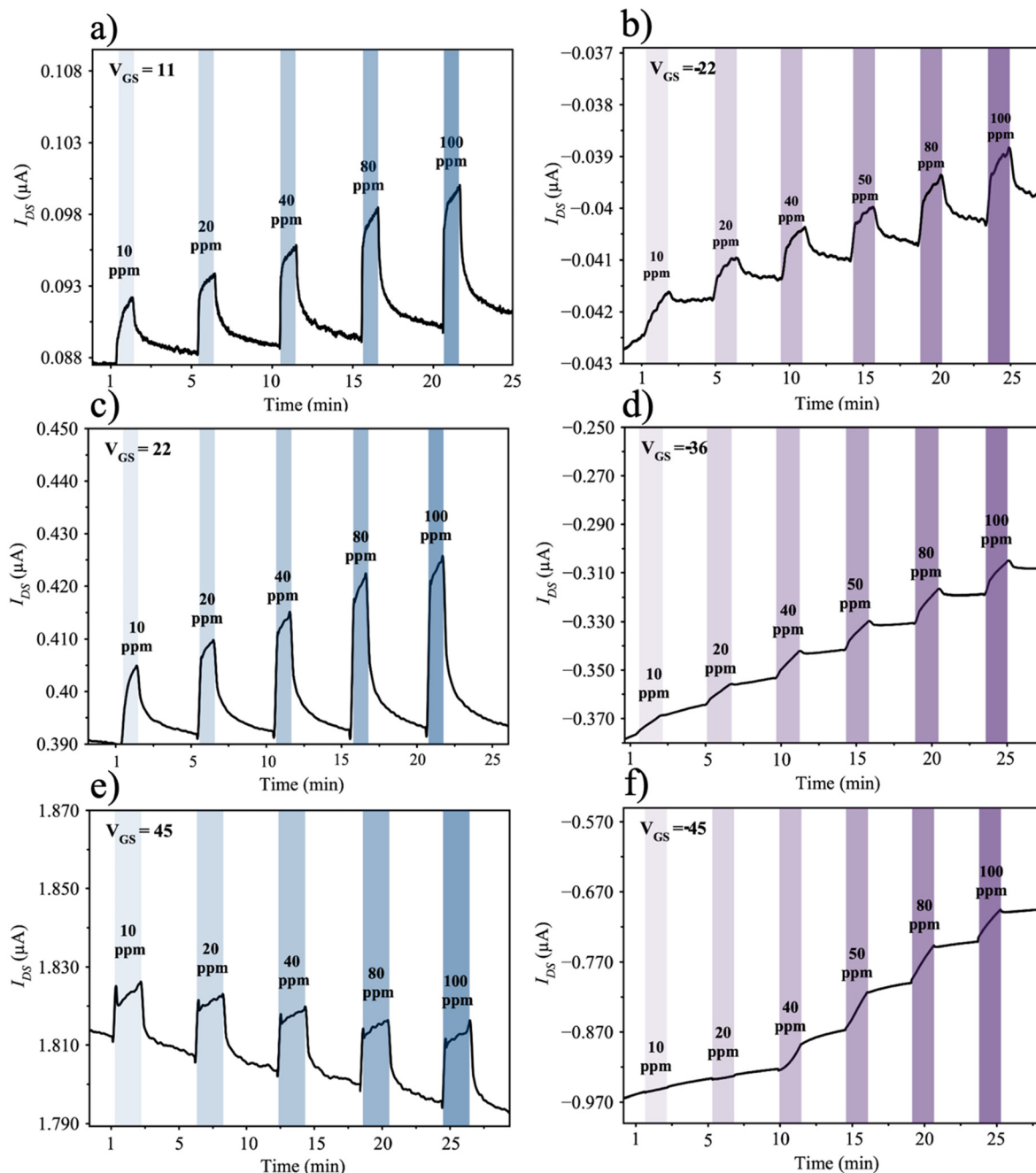
Fig. 4 Response of OTFT sensors under successive exposure of NH₃ for 1 min and recovery under synthetic air for 4 min in the range of NH₃ concentration from 10–100 ppm in dry air and 20–22° at different V_{GS}. a), c) and e) F_{16}CuPc OTFT and b), d) and f) CuPc OTFT. For F_{16}CuPc, a $V_{DS} = 45$ V was used for all the measurements and for CuPc, $V_{DS} = -45$ V.

sensor displayed a linear and enhanced response, achieving a maximum sensitivity of 0.024% per ppm, three orders of magnitude higher than previously reported for chemiresistor configurations.[28] Further reduction in V_{GS} to −22 V did not yield significant changes in sensitivity, suggesting saturation in this regime (Table 1).

In contrast, F_{16}CuPc OTFT sensors demonstrated linear behavior across all gate biases, with notable improvement at lower V_{GS}. At $V_{GS} = 11$ V, sensitivity increased by a factor of 33 compared to operation at 45 V. This strong gate dependence

underscores the tunability of OTFT-based sensors for optimizing performance parameters.

To estimate the minimum detectable concentration, the LOD was calculated using eqn (3).[33]

$$\text{LOD} = \frac{3N}{S \times I_0} \quad (3)$$

where N is the standard deviation of the baseline current during the recovery period, S is sensitivity (ppm⁻¹), and I_0 is the baseline current. The extracted LOD values are presented in Table 1.

Table 1 Summary of gas sensing parameters as a function of V_{GS} for CuPc and F_{16}CuPc OTFT-based sensors

Semiconductor	V_{GS} (V)	S^a (% per ppm)	LOD^b (ppm)	Res. time^c (s)	Rec. time^c (s)
CuPc	22	−0.01	4.73	40.04	N/A
	36	−0.02^d	0.40^d	57.51	N/A
	45	N/A	N/A	60.08	N/A
F_{16}CuPc	11	0.1	0.53	30.70	180.52
	22	0.07	0.21	40.10	113.79
	45	0.003	1.042	33.76	102.98

^{a} Sensitivity (S) is expressed as the percentage change in current per ppm of NH_3. ^{b} LOD was calculated according to eqn (3). ^{c} Response (Res) and recovery (Rec) times correspond to the time to reach 90% signal change. N/A indicates cases where the current did not recover to 90% of its initial value or the value could not be calculated. ^{d} Under these conditions, no recovery was observed for the sensor upon exposure to NH_3.

Interestingly, although sensitivity decreases with increasing V_{GS}, lower LOD values are achieved at higher gate biases due to the larger baseline currents, which improves the signal-to-noise ratio. For CuPc, the LOD improved from 4.73 ppm at V_{GS} = −22 V to 0.4 ppm at V_{GS} = −36 V. However, it is important to mention that the CuPc sensor operated at V_{GS} = −36 V and V_{GS} = −45 V don't show an appropriate recovery after exposure, limiting its sensing capabilities. Therefore, the values calculated for LOD and sensitivity are mentioned only for comparison reasons. A similar trend was observed for F_{16}CuPc, where the LOD decreased from 1.04 ppm at V_{GS} = 45 V to 0.21 ppm at V_{GS} = 22 V. As V_{GS} directly modulates the current in the OTFT architecture, the LOD can be tuned accordingly depending on the sensor's application. By adjusting the gate bias, the sensor's baseline current and amplification characteristics change, enabling optimization for either high sensitivity or low detection thresholds based on specific environmental or industrial needs.

Baseline drift remains a critical challenge in the practical deployment of OTFT-based gas sensors, often limiting device stability and long-term reliability even for encapsulated OTFTs.[34,35] This drift is primarily associated with incomplete desorption of analytes during the recovery phase, as well as charge trapping effects induced by prolonged gate bias. While strategies such as thermal desorption or pulsed gating have been shown to mitigate drift in various FET-based sensing platforms,[36] they typically require additional circuitry or temperature control that complicate device integration. In contrast, our results demonstrate that modulation of the gate voltage alone can mitigate baseline drift in OTFT sensors operating at room temperature, offering a practical and low-power approach for performance enhancement.

Recovery and response times were calculated from the same short-exposure experiments used to evaluate sensitivity and LOD. The response time is defined here as the time required for the drain current I_{DS} to reach 90% of its maximum value after exposure to NH_3, while the recovery time corresponds to the time required for I_{DS} to return to 90% of its baseline following analyte removal. In both CuPc and F_{16}CuPc-based sensors, the response time showed limited dependence on gate bias. For F_{16}CuPc OTFT sensors, the response time ranged from 30.7 s at V_{GS} = 11 V to 33.76 s

at V_{GS} = 45 V, indicating minimal influence of gate modulation on the response dynamics. CuPc OTFT sensors showed a slightly different behavior, where the fastest response (40.04 s) was observed at the lowest measured V_{GS} of 22 V.

Recovery behavior exhibited a clear dependence on gate bias, particularly for F_{16}CuPc-based sensors. At V_{GS} = 11 V, a positive drift in baseline current was observed (Fig. 4e), likely due to incomplete NH_3 desorption. Despite this, the sensor successfully returned to 90% of its baseline signal within a recovery time of 180.52 s, indicating effective recovery even under low gate bias conditions. When operated at V_{GS} = 45 V, the baseline drift reversed to a negative direction (Fig. 4c), likely reflecting stronger bias stress effects; however, the recovery was faster, reaching 90% recovery in 102.98 s. Notably, at an intermediate bias of V_{GS} = 22 V, the sensor exhibited minimal drift and a recovery time of 113.79 s. This intermediate behavior suggests a compensatory effect in which incomplete desorption and electrical stress-induced degradation balance out.

CuPc-based sensors, in contrast, did not reach 90% recovery within the measurement window at any applied V_{GS}. The baseline drift was consistently negative, indicating persistent charge trapping and limited desorption. Notably, operating at lower V_{GS} values reduced the extent of current drift (Fig. 4b and d), suggesting reduced bias stress, but this was not sufficient to enable full recovery. These results reinforce the material-dependent nature of OTFT sensor recovery, highlighting the role of semiconductor–analyte interactions and electrical stress tolerance.

4. Conclusion

We successfully fabricated highly sensitive OTFT-based NH_3 sensors employing CuPc and F_{16}CuPc as the sensing layer for the first time and systematically investigated the influence of V_{GS} on their response kinetics and detection limit. Modulation of V_{GS} proved to be a simple yet highly effective approach to enhance sensor characteristics for both materials. Specifically, reducing V_{GS} significantly improved the sensitivity of F_{16}CuPc sensors, increasing by a factor of 33 when switching the V_{GS} from 45 V to 11 V, reaching a maximum sensitivity of 0.1 (% per ppm). For CuPc sensors,

the RR to low NH_3 concentrations (10 and 20 ppm) was initially negligible but was improved to 2.1% and 2.3%, respectively, achieving a maximum sensitivity of 0.02 (% per ppm). We also demonstrate that the LOD was also influenced by tuning the V_{GS}, where a larger applied V_{GS} yielded lower LOD values, with CuPc exhibiting a reduction by an order of magnitude 4.73 ppm to 0.4 ppm, and $F_{16}CuPc$ displaying a twofold decrease from 0.5 ppm to 0.2 ppm. This improvement is attributed to an enhanced signal-to-noise ratio, which can be finely controlled through V_{GS} modulation in OTFT architectures.

We also demonstrated the response and recovery kinetics were influenced by the V_{GS}. CuPc-based devices showed moderate response times (40–60 s), but failed to recover 90% of their initial current after NH_3 exposure. In contrast, $F_{16}CuPc$ devices exhibited faster response times (31–40 s) and significantly better recovery, with 90% current recovery in 103 s by increasing the V_{GS} from 11 to 45 V. These differences were related to the baseline drift and adsorption–desorption behaviors specific to each material. Overall, this work highlights V_{GS} modulation as a powerful strategy to improve the sensitivity and dynamic response of OTFT-based gas sensors and provides a highly effective pathway for the design of highly tunable, application-oriented sensing platforms.

Conflicts of interest

There are no conflicts to declare.

Data availability

Supplementary information presenting all the mobility and threshold voltage values for both semiconductors under different ammonia concentrations and the fittings for the sentivity calculations is available here. See DOI: https://doi.org/10.1039/D5SD00103J.

All data necessary to support the conclusions of this study are provided in the manuscript and the SI. Additional information is available from the corresponding author upon reasonable request.

Acknowledgements

References

1 A. Rothschild and Y. Komem, The effect of grain size on the sensitivity of nanocrystalline metal-oxide gas sensors, *J. Appl. Phys.*, 2004, **95**(11), 6374–6380, DOI: 10.1063/1.1728314.

2 S. Kiruba Mangalam, A. S. Jose, K. Prajwal, P. Chowdhury and H. C. Barshilia, Sputter deposited p-NiO/n-SnO2 porous thin film heterojunction based NO2 sensor with high selectivity and fast response, *Sens. Actuators, B*, 2020, **310**, 127830, DOI: 10.1016/j.snb.2020.127830.

3 S. Maheswari, M. Karunakaran, K. Kasirajan, L. Bruno Chandrasekar and P. Boomi, Yttrium - Substituted SnO2 thin films and its gas sensing activity against NH3 gas: Characterization and sensitivity evaluation, *Sens. Actuators, A*, 2020, **315**, 112303, DOI: 10.1016/j.sna.2020.112303.

4 A. K. Singh, N. K. Chowdhury, S. C. Roy and B. Bhowmik, Review of Thin Film Transistor Gas Sensors: Comparison with Resistive and Capacitive Sensors, *J. Electron. Mater.*, 2022, **51**(5), 1974–2003, DOI: 10.1007/s11664-022-09485-y.

5 S. Khan, S. Ali and A. Bermak, Recent Developments in Printing Flexible and Wearable Sensing Electronics for Healthcare Applications, *Sensors*, 2019, **19**(5), 1230, DOI: 10.3390/s19051230.

6 A. Kumar, R. Meunier-Prest, E. Lesniewska and M. Bouvet, Interplay of electrode geometry and bias on charge transport in organic heterojunction gas sensors, *Sens. Actuators, B*, 2022, **369**, 132313, DOI: 10.1016/j.snb.2022.132313.

7 G. Bengasi, R. Meunier-Prest and K. Baba, *et al.*, Molecular Engineering of Porphyrin-Tapes/Phthalocyanine Heterojunctions for a Highly Sensitive Ammonia Sensor, *Adv. Electron. Mater.*, 2020, **6**(12), 2000812, DOI: 10.1002/aelm.202000812.

8 C. Zhang, K. Xu, K. Liu, J. Xu and Z. Zheng, Metal oxide resistive sensors for carbon dioxide detection, *Coord. Chem. Rev.*, 2022, **472**, 214758, DOI: 10.1016/j.ccr.2022.214758.

9 L. Di Zazzo, S. Ganesh Moorthy and R. Meunier-Prest, *et al.*, Ammonia and Humidity Sensing by Phthalocyanine–Corrole Complex Heterostructure Devices, *Sensors*, 2023, **23**(15), 6773, DOI: 10.3390/s23156773.

10 V. Ivanova, D. Klyamer and G. Tunç, *et al.*, Films of substituted zinc phthalocyanines as active layers of chemiresistive sensors for ammonia detection, *New J. Chem.*, 2023, **47**(42), 19633–19645, DOI: 10.1039/D3NJ03400C.

11 B. King, S. G. Moorthy, E. Lesniewska, R. Meunier-Prest, M. Bouvet and B. H. Lessard, Modulating the majority charge carrier type and performance of organic heterojunction ammonia sensors by increasing peripheral fluorination of the silicon phthalocyanine sublayer, *Sens. Actuators, B*, 2024, **408**, 135507, DOI: 10.1016/j.snb.2024.135507.

12 L. Van Duy, T. Thi Nguyet and C. M. Hung, *et al.*, Light-assisted room temperature ammonia gas sensor based on porphyrin-coated V2O5 nanosheets, *Sens. Actuators, B*, 2024, **409**, 135582, DOI: 10.1016/j.snb.2024.135582.

13 F. Yan and H. Tang, Application of thin-film transistors in label-free DNA biosensors, *Expert Rev. Mol. Diagn.*, 2010, **10**(5), 547–549, DOI: 10.1586/erm.10.50.

14 B. Shao, Y. Liu and X. Zhuang, *et al.*, Crystallinity and grain boundary control of TIPS-pentacene in organic thin-film transistors for the ultra-high sensitive detection of NO2, *J. Mater. Chem. C*, 2019, **7**(33), 10196–10202, DOI: **10.1039/C9TC01219B**.

15 Z. Song, G. Liu, Q. Tang, X. Zhao, Y. Tong and Y. Liu, Controllable gas selectivity at room temperature based on Ph5T2-modified CuPc nanowire field-effect transistors, *Org. Electron.*, 2017, **48**, 68–76, DOI: **10.1016/j.orgel.2017.05.043**.

16 S. Ganesh Moorthy, B. King, A. Kumar, E. Lesniewska, B. H. Lessard and M. Bouvet, Molecular Engineering of Silicon Phthalocyanine to Improve the Charge Transport and Ammonia Sensing Properties of Organic Heterojunction Gas Sensors, *Adv. Sens. Res.*, 2023, **2**(3), 2200030, DOI: **10.1002/adsr.202200030**.

17 E. Singh, M. Meyyappan and H. S. Nalwa, Flexible Graphene-Based Wearable Gas and Chemical Sensors, *ACS Appl. Mater. Interfaces*, 2025, **9**(39), 34544–34586, DOI: **10.1021/acsami.7b07063**.

18 F. Wen, D. C. Dillen, K. Kim and E. Tutuc, Shell morphology and Raman spectra of epitaxial Ge−SixGe1−x and Si−SixGe1−x core-shell nanowires, *J. Appl. Phys.*, 2017, **121**(23), 234302, DOI: **10.1063/1.4985616**.

19 W. Shi, J. Yu and H. E. Katz, Sensitive and selective pentacene-guanine field-effect transistor sensing of nitrogen dioxide and interferent vapor analytes, *Sens. Actuators, B*, 2018, **254**, 940–948, DOI: **10.1016/j.snb.2017.07.198**.

20 W. Huang, X. Zhuang and F. S. Melkonyan, *et al.*, UV–Ozone Interfacial Modification in Organic Transistors for High-Sensitivity NO2 Detection, *Adv. Mater.*, 2017, **29**(31), 1701706, DOI: **10.1002/adma.201701706**.

21 A. G. Santos, G. O. da Rocha and J. B. de Andrade, Occurrence of the potent mutagens 2- nitrobenzanthrone and 3-nitrobenzanthrone in fine airborne particles, *Sci. Rep.*, 2019, **9**(1), 1, DOI: **10.1038/s41598-018-37186-2**.

22 Y. Jiang, W. Huang, X. Zhuang, Y. Tang and J. Yu, Thickness modulation on semiconductor towards high performance gas sensors based on organic thin film transistors, *Mater. Sci. Eng., B*, 2017, **226**, 107–113, DOI: **10.1016/j.mseb.2017.08.019**.

23 Y. Sato, K. Takai and T. Enoki, Electrically controlled adsorption of oxygen in bilayer graphene devices, *Nano Lett.*, 2011, **11**(8), 3468–3475, DOI: **10.1021/nl202002p**.

24 S. S. Shetty, A. Jayarama, S. Bhat, Satyanarayan, I. Karunasagar and R. Pinto, A review on metal-oxide based trace ammonia sensor for detection of renal disease by exhaled breath analysis, *Mater. Today: Proc.*, 2022, **55**, 113–117, DOI: **10.1016/j.matpr.2021.12.411**.

25 Ammonia: zero-carbon fertiliser, fuel and energy store.

26 L. S. Chia, Y. H. Du, S. Palale and P. S. Lee, Interaction of Copper Phthalocyanine with Nitrogen Dioxide and Ammonia Investigation Using X-ray Absorption Spectroscopy and Chemiresistive Gas Measurements, *ACS Omega*, 2019, **4**(6), 10388–10395, DOI: **10.1021/acsomega.8b02108**.

27 N. T. Boileau, O. A. Melville, B. Mirka, R. Cranston and B. H. Lessard, P and N type copper phthalocyanines as effective semiconductors in organic thin-film transistor based DNA biosensors at elevated temperatures, *RSC Adv.*, 2019, **9**(4), 2133–2142, DOI: **10.1039/C8RA08829B**.

28 L. S. Chia, Y. H. Du, S. Palale and P. S. Lee, Interaction of Copper Phthalocyanine with Nitrogen Dioxide and Ammonia Investigation Using X-ray Absorption Spectroscopy and Chemiresistive Gas Measurements, *ACS Omega*, 2019, **4**(6), 10388–10395, DOI: **10.1021/acsomega.8b02108**.

29 W. Huang, K. Besar, R. LeCover, A. M. Rule, P. N. Breysse and H. E. Katz, Highly sensitive NH3 detection based on organic field-effect transistors with tris(pentafluorophenyl) borane as receptor, *J. Am. Chem. Soc.*, 2012, **134**(36), 14650–14653, DOI: **10.1021/ja305287p**.

30 H. Fan, W. Shi, X. Yu and J. Yu, High performance nitrogen dioxide sensor based on organic field-effect transistor utilizing ultrathin CuPc/PTCDI-C8 heterojunction, *Synth. Met.*, 2016, **211**, 161–166, DOI: **10.1016/j.synthmet.2015.11.021**.

31 M. Mateos, R. Meunier-Prest, J. M. Suisse and M. Bouvet, Modulation of the organic heterojunction behavior, from electrografting to enhanced sensing properties, *Sens. Actuators, B*, 2019, **299**, 126968, DOI: **10.1016/j.snb.2019.126968**.

32 R. B. Ewenike, B. King and A. M. Battaglia, *et al.*, Toward Weak Epitaxial Growth of Silicon Phthalocyanines: How the Choice of the Optimal Templating Layer Differs from Traditional Phthalocyanines, *ACS Appl. Electron. Mater.*, 2023, **5**(12), 7023–7033, DOI: **10.1021/acsaelm.3c01389**.

33 B. King and B. H. Lessard, Review of recent advances and sensing mechanisms in solid-state organic thin-film transistor (OTFT) sensors, *J. Mater. Chem. C*, 2024, **12**(16), 5654–5683, DOI: **10.1039/D3TC03611A**.

34 H. F. Haneef, A. M. Zeidell and O. D. Jurchescu, Charge carrier traps in organic semiconductors: a review on the underlying physics and impact on electronic devices, *J. Mater. Chem. C*, 2020, **8**(3), 759–787, DOI: **10.1039/C9TC05695E**.

35 S. J. Zilker, C. Detcheverry, E. Cantatore and D. M. de Leeuw, Bias stress in organic thin-film transistors and logic gates, *Appl. Phys. Lett.*, 2001, **79**(8), 1124–1126, DOI: **10.1063/1.1394718**.

36 R. D. Yang, J. Park, C. N. Colesniuc, I. K. Schuller, W. C. Trogler and A. C. Kummel, Ultralow drift in organic thin-film transistor chemical sensors by pulsed gating, *J. Appl. Phys.*, 2007, **102**(3), 034515, DOI: **10.1063/1.2767633**.